Characterization of turbulent coherent structures in square duct flow

IOP Conf. Series: Journal of Physics: Conf. Series **1001** (2018) 012008 doi:10.1088/1742-6596/1001/1/012008

Characterization of turbulent coherent structures in square duct flow

Marco Atzori[1], Ricardo Vinuesa[1], Adrián Lozano-Durán[2] and Philipp Schlatter[1]

[1] Linné FLOW Centre, KTH Mechanics, SE-100 44 Stockholm, Sweden and Swedish e-Science Research Centre (SeRC), Stockholm, Sweden
[2] Center for Turbulence Research, Stanford, CA, USA

E-mail: atzori@mech.kth.se

Abstract. This work is aimed at a first characterization of coherent structures in turbulent square duct flows. Coherent structures are defined as connected components in the domain identified as places where a quantity of interest (such as Reynolds stress or vorticity) is larger than a prescribed non-uniform threshold. Firstly, we qualitatively discuss how a percolation analysis can be used to assess the effectiveness of the threshold function, and how it can be affected by statistical uncertainty. Secondly, various physical quantities that are expected to play an important role in the dynamics of the secondary flow of Prandtl's second kind are studied. Furthermore, a characterization of intense Reynolds-stress events in square duct flow, together with a comparison of their shape for analogous events in channel flow at the same Reynolds number, is presented.

1. Introduction

The interest in the description of duct flows originates both from practical applications (ducts are widely used in cooling systems, for instance) and from the presence of the secondary flow of Prandtl's second kind. This phenomenon, despite representing only around 2 to 3% of the bulk velocity [1], has an important impact in the wall-shear stress distribution along the perimeter of the duct. In duct flows, the simulations by Gavrilakis [2] revealed the emergence of eight counter-rotating vortices which convect momentum from the core of the duct to its bisector. More recently, Pinelli *et al.* [3] reported that the secondary flow has contributions both from the large-scale motions and from the near-wall region of turbulence.

In the present study the considered data sets are part of the direct numerical simulation (DNS) data of turbulent duct flow by Vinuesa *et al.* [4, 5] and the DNS of turbulent channel flow employed by del Álamo *et al.* [6]. We focus on square duct and channel both at a friction Reynolds number Re_τ of 180. The friction Reynolds number Re_τ is computed based on the half-height and the friction velocity $u_\tau = \sqrt{\tau_w/\rho}$ (τ_w is the wall-shear stress and ρ the density of the fluid). For the duct, we will define Re_τ in terms of the centerplane friction velocity. We consider a frame of reference with the x, y and z axes aligned with the streamwise, wall-normal and spanwise directions of the channel, respectively. An analogous frame of references is adopted for the duct, but it has to be noted that in this case the y and z directions are equivalent given the symmetry of the problem. The instantaneous velocity components are denoted as $\tilde{u}$, $\tilde{v}$ and $\tilde{w}$, while the mean and the fluctuating components are respectively U, V and W and

u, v and w. Root-mean-squares are indicated explicitly. The aim of the present study is to

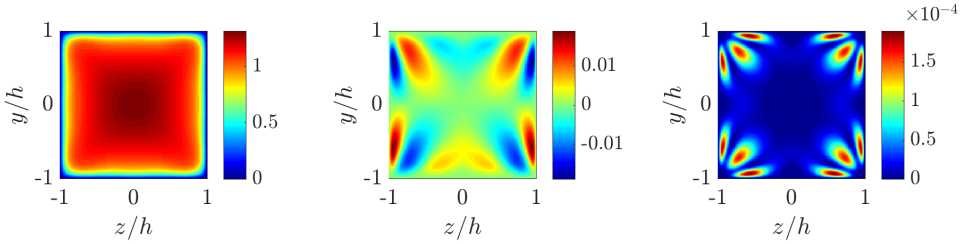

Figure 1. From left to right: average of the streamwise velocity component U, of the vertical component V and of kinetic energy of the secondary flow $K = 1/2(V^2 + W^2)$ for square duct flow at $Re_\tau = 180$ at the centerplane.

extend our knowledge regarding the phenomenology of duct flows by describing the behavior of the coherent turbulent structures present in the flow. In our analysis we will follow the same procedure applied by del Álamo *et al.* [6] and Lozano-Durán *et al.* [7] for channel flows.
To identify three-dimensional structures implies finding connected components of the computational domain that fulfill a certain condition for a quantity of interest. *Vortex clusters*, first analyzed in turbulent channel flows by del Álamo *et al.* [7], denote regions of the flow where strain is small compared with the vorticity and the local pressure is low. In this case the physical quantity of interest can be, for instance, the second invariant of $\nabla\mathbf{u}$, Q, as proposed by Hunt *et al.* [8]

$$Q = \frac{1}{2}\left(\frac{\partial^2 u_i}{\partial x_i^2} - \frac{\partial u_i}{\partial x_j}\frac{\partial u_j}{\partial x_i}\right). \tag{1}$$

Other options are the λ_2 criterion (Jeong and Hussain [9]) and the Δ criterion (Chong *et al.* [10]). Chakraborty *et al.* [11] showed that all these methods are approximately equivalent, which strongly suggestes that the choice of a particular criterion does not affect the results. Despite the fact that for these criteria a threshold of 0 is the most natural choice, it tends to include a very large fraction of the overall volume of the domain. Therefore, a scalar value, initially prescribed *ad hoc*, is preferred (Chong *et al.* [12]). However, as firstly suggested by Nagaosa and Handler [13], in non-homogeneous flows the threshold should be such that the varying magnitude of the fluctuations in different regions of the flow is taken into account. To this end, they proposed for the identification of vortex clusters to scale Q with its local root-mean-square value. Thus, the condition for belonging to a connected component becomes:

$$Q = \beta\, Q_{rms}. \tag{2}$$

The choice of β remained relatively subjective, until Moisy and Jiménez [14] introduced the percolation analysis to obtain a quantitative measurement of the effects of different thresholds. Subsequently, del Álamo *et al.* [6] and Lozano-Durán *et al.* [7] adopted the same procedure. In the latter study the authors also considered regions with high Reynolds-stress events, by performing a three-dimensional extension of the *quadrant analysis*. The quadrant analysis was originally proposed by Wallace *et al.* [15] and employed by Willmarth and Lu [16] as an experimental technique for the detection of burst and sweep events, which are identified via a simultaneous measurement of u and v, and Lu and Willmarth [17] introduced a threshold based on the root-mean-square of these components to identify more intense events, leading to the following condition

$$|uv| > H_{uv}\, u_{rms} v_{rms}. \tag{3}$$

Here H is the so-called *hyperbolic hole*, which has the graphical interpretation of the region excluded by the hyperbola $|uv| = H$ in the Cartesian plane u,v, where different quadrants correspond to various events: $u > 0$ and $v > 0$ are outward interactions ($Q1$), $u < 0$ and $v > 0$ ejections ($Q2$), $u < 0$ and $v < 0$ inward interactions ($Q3$) and $u > 0$ and $v < 0$ are sweeps ($Q4$). The similarities between equations (2) and (3) inspires the adoption of the latter equation to detect three-dimensional structures which correspond to the four quadrants, as indeed done by Lozano-Durán *et al.* [7], who also employed the percolation analysis for the choice of H (as done for β in del Álamo *et al.* [6]). One of the main findings from these studies is the fact that the predominant structure in the logarithmic layer of wall-bounded flows is a $Q2 - Q4$ pair, which is associated with a vortex cluster [7]. Our main purpose is to extend this analysis to other kind of structures. Moreover, we clarify some details regarding the detection procedure, with the aim of extending its application and robustness for other flow configurations.

2. Structure identification method

2.1. Role of the percolation analysis

The role of the percolation analysis in the structure identification method deserves specific attention. Here we consider a simple test case to clarify how it can be employed in order to estimate an adequate threshold for a data-set containing several snapshots of non-homogeneous turbulent flows. Firstly, let us consider a square two-dimensional lattice, where the probability of a site of the lattice being occupied or not is defined by p. A certain definition of connectivity among occupied sites is also provided, for instance, between nearest neighbors. If one considers increasing values of p starting from 0, it will be possible to observe the existence of a critical p_c, above which most of the existing small connected components merge into less numerous but larger ones. This phenomenon is called *percolation crisis*. Let us introduce a scalar field $f(x, y)$ defined on a certain grid (we maintain a two-dimensional frame for the sake of simplicity), and the grid points satisfying the following condition are identified

$$f(x, y) > \alpha. \tag{4}$$

In this example, grid points are equivalent to sites of the lattice and p represents the probability for each point to fulfill condition (4), thus the percolation is determined by the properties of f. Here we focus on three particular cases: a) f is a stochastic variable uniformly distributed between 0 and 1; b) f is a stochastic variable with a Gaussian distribution of zero mean and a standard deviation of 1/2; c) f is defined as a uniformly distributed stochastic variable denoted as $U(a, b)$, where a and b are the minimum and maximum values, added to a linear function (*e.g.*: the coordinate y), so that $0 < f < 1$ still holds. An example could be

$$f = U\left(0, 1/2\right) + \frac{y}{2(y_{\max} - y_{\min})}. \tag{5}$$

If f is homogeneously distributed, the merging process takes place simultaneously in the whole domain and it is possible to identify a short interval of values of α where it occurs. On the other hand, if f is not homogeneous, the percolation exhibits a different behavior because the merging process cannot occur at the same time in the whole domain. Instead, it proceeds *expanding* the connected components from the region where f is lower to the regions there f is higher. The process is more gradual and it is not possible to clearly identify the interval of values of α where most of the merging processes takes place. In order to clarify these concepts, let us define $V^*(\alpha)$ and $N^*(\alpha)$ as the ratio of the volume of the largest structure divided by the total volume occupied by all the structures, and the total number of objects normalized with the largest number of identified objects over all the values of α, respectively. In addition, we also introduce α_c, which is the value where the derivative $\mathrm{d}V^*/\mathrm{d}\alpha$ is minimum (this would be the

value of α for which the merging process is most intense), and $\alpha_{\max}$, which is value that produces the highest number of objects. Figure 2 shows the percolation analysis for the three different test cases introduced above. Only for cases a) and b), represented by solid and dashed lines respectively, it is possible to identify unambiguously α_c and $\alpha_{\max}$, while it is not possible for case c), represented by dotted lines. In Figure 2 it is also possible to observe the difference between cases a) and b). In the first case, since $f \in [0, 1]$, for $\alpha = 1$ no grid points fulfill condition (4), therefore $N(1) \simeq 0$. By contrast, in case c) it is possible to have points with $f > 1$ which are always above α, thus $N(1) > 0$. These examples allow us to identify the first role of the

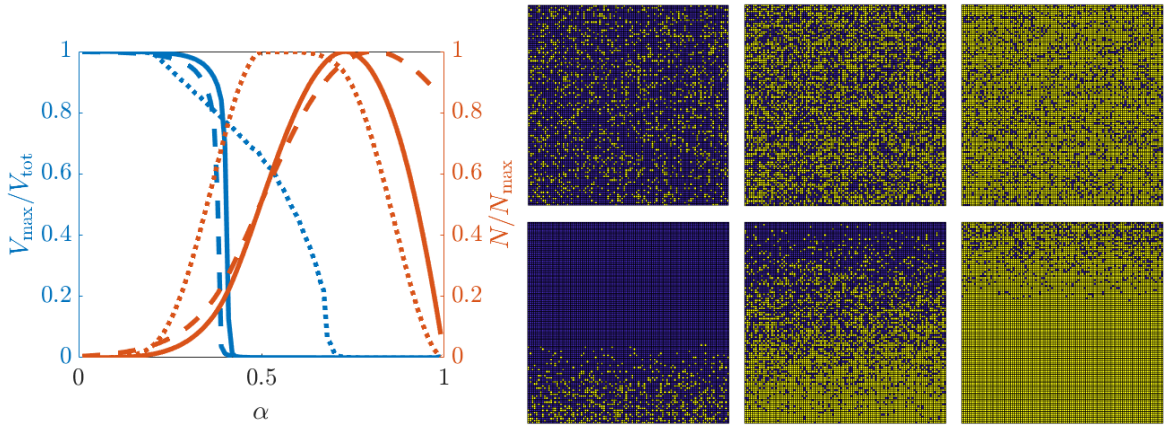

Figure 2. Percolation analysis for a square two-dimensional domain. (Left) The $V^*(\alpha)$ and $N^*(\alpha)$ curves are represented in blue and red, respectively. Solid lines correspond to the uniformly distributed case, dashed lines to the case with a Gaussian distribution and dotted lines denote the case with the addition of a linear function as in equation (5). (Right) Connected components (in yellow) identified in the grid corresponding to (top) solid and (bottom) dotted lines on left panel. The values of α are, from left to right, 0.8, 0.5 and 0.3.

percolation analysis in detecting coherent structures. Conditions such as equations (2) or (3) are equivalent to the general form $f > \alpha$ if Q and $|uv|$ are scaled with factors obtained from the flow statistics of the threshold function, while β and H play the role of α. A sharp percolation crisis obtained when gradually modifying the value of β (or H) indicates that the threshold function is able to capture the non-homogeneity of the flow properly.

It is also important to take into account the influence of the size of the domain on the percolation analysis, which is related to the uncertainty of the statistics. Regarding flow statistics, if boundary effects are negligible, to employ a larger computational domain is equivalent to consider a larger data set. This is not obvious for the percolation analysis, since in a finite domain both the largest possible number of observed structures and the size of the largest structure are bounded and related to the size of the domain itself. To qualitative estimate these effects, we limit our analysis to the case of a uniformly distributed random field without superimposed bias (case a) introduced above) and we consider 50 snapshots for three different sizes of the square grid (25×25, 100×100 and 500×500). For each of these data-sets, the percolation analysis is performed via averaging each value of V^* and N^* for the prescribed α. As shown in Figure 3, smaller domains lead to a wider range of values of α over which the percolation crisis takes place, a fact that increases the uncertainty in the estimation of $\alpha_{\max}$ and α_c. However, the values of α_c and $\alpha_{\max}$ resulting from the averages are consistent for all the considered sizes. This result is of great interest since the typical data-set considered in this analysis consists of a collection of instantaneous flow fields which have at least one direction of periodicity. This result therefore

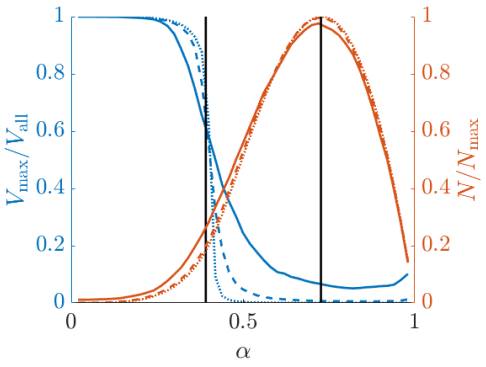

Figure 3. Percolation analysis averaged over 50 snapshots of square two-dimensional domains of different sizes. The $V^*(\alpha)$ and $N^*(\alpha)$ curves are represented in blue and red, respectively, and the solid, dashed and dotted lines represent the cases with 25×25, 100×100 and 500×500 grid points. The two vertical black lines represent α_c and $\alpha_{\max}$. Note that for the averaged curves, α_c and $\alpha_{\max}$ are identical in the three domain sizes.

justifies the employment of the percolation analysis to identify the optimal value of β (or H) that maximizes the number of detected objects for a certain case, which is the second role of the percolation analysis in this context.
Based on the results of the simple test cases presented above, it is possible to summarize how the percolation analysis is employed in the present work. Firstly, it is employed to evaluate the effectiveness of the threshold functions in identifying simultaneously coherent structures in the whole domain. And secondly, it is used to estimate the value of β (or H) which maximizes the number of detected objects.

2.2. Flow structures under consideration
The first coherent structures under study are the intense Reynolds stresses, uv, which have been extensively studied by Lozano-Durán *et al.* [7] and Lozano-Durán and Jiménez [18] in turbulent channel flows. As mentioned above, their threshold function was the same as that employed by Lu and Willmarth [17], resulting in the condition given by equation (3). Inspection of the structures obtained using this condition without additional corrections revealed that the near-wall region remained occupied by large structures for higher H than the rest of the domain. Considering the relatively low Reynolds number under consideration, we attribute this observation to the large outer-scaled wall-normal extent of the viscous sublayer, which results in a relatively large region where $u_{rms}v_{rms}$ is too low to work effectively as a threshold. In this case, we propose as a solution to modify the threshold function via substituting the threshold values below $y^+ = 5$ with the one at $y^+ = 5$. The effect of this correction on the percolation curve is shown in Figure 4 and we conclude that it improves the percolation behavior in the context of the present work.
Because of the geometry of the duct, uv events are equivalent to uv events in turbulent channels only with respect to the top and bottom walls, while they correspond to cross-flow events on the left and right walls. Moreover, in the square duct the uw events on the side walls are analogous to the uv on the horizontal walls due to the symmetry, and in the present work we identify them by applying the condition

$$|uw| > H_{uw}\, u_{rms} w_{rms}. \tag{6}$$

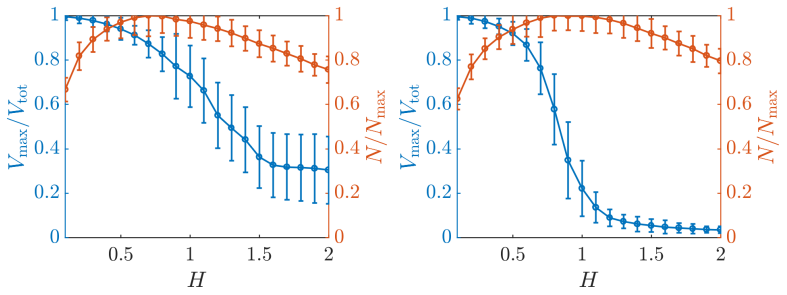

Figure 4. Percolation analysis for uv. Curves obtained (left) without and (right) with a correction for grid points below $z^+, y^+ = 5$.

Note that the percolation analysis is also analogous to the one for uv structures, and therefore it is not shown here. The present analysis is extended to other structures by considering three different quantities that are related to the secondary flow of Prandtl's second kind. The first natural candidate is the Reynolds-shear stress term vw. As in the analysis performed for the uv and uw structures, we adopted the condition

$$|vw| > H_{vw}\, v_{rms} w_{rms} \tag{7}$$

for the vw structures. The resulting percolation analysis is shown in Figure 5 (left), where essentially the same trend as that observed for the uv structures in Figure 4 is obtained. An additional coherent structure that we take into consideration corresponds to intense regions of the normal Reynolds-stress difference $|v^2 - w^2|$. Note that this type of coherent structure is analyzed due to its role in the streamwise vorticity transport equation, see for instance Ref. [18]. The choice of the threshold in this case is less obvious. Since the values of v^2_{rms} and w^2_{rms} are almost equal in the core of the duct and along the diagonals, differences such as $|v^2_{rms} - w^2_{rms}|$ cannot be used as a threshold because they are close to 0 in a large portion of the domain. Considering that the difference $|v^2 - w^2|$ exhibits the highest values close the walls, where v^2 is larger than w^2 (in the case of vertical walls) – or vice-versa (when considering horizontal walls), we propose the sum $v^2_{rms} + w^2_{rms}$, which is of the order of the largest quantities near the walls and of each individual term elsewhere. The percolation condition is therefore

$$|v^2 - w^2| > H_{v^2-w^2}\, (v^2_{rms} + w^2_{rms}), \tag{8}$$

which provides similar percolation trends as the ones observed in the uv and vw structures, as shown in Figure 5 (center). We also consider an additional type of structure, defined by connected regions of high K, the instantaneous kinetic energy of the secondary flow defined by Vinuesa *et al.* [19]. Despite the fact that K is calculated in terms of to the instantaneous velocity components $\tilde{v}$ and $\tilde{w}$ instead of their fluctuations, the following condition constitutes an effective threshold, as shown in Figure 5 (right)

$$K = \frac{1}{2}\left(\tilde{v}^2 + \tilde{w}^2\right) > H_K\, \frac{1}{2}(v^2_{rms} + w^2_{rms}). \tag{9}$$

Before proceeding with the analysis of the turbulent structures, it is important to note that the choice of an adequate threshold for a generic field requires further investigation. Let us consider, as an example, two alternative conditions for the detection of uv events

$$|uv| > H'_{uv}\frac{1}{2}\left(u^2_{rms} + v^2_{rms}\right), \qquad |uv| > H''_{uv}\frac{1}{2}\left(u^2_{rms} + v^2_{rms} + w^2_{rms}\right). \tag{10}$$

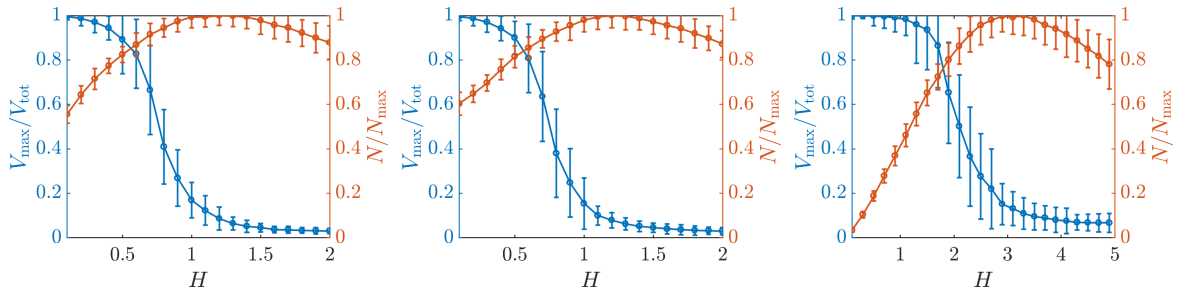

Figure 5. Percolation analysis for (left) vw, for (center) $|v^2-w^2|$ and (right) $K=1/2(\tilde{v}^2+\tilde{w}^2)$.

As shown in Figure 6, in both the cases the percolation analysis gives a very similar outcome to that obtained with $|uv| > H_{uv}\, u_{rms} v_{rms}$. This shows, on the one hand, that the percolation crisis should be considered as a necessary but not sufficient condition for the acceptance of a certain threshold function, and on the other hand that a more rigorous procedure might be needed to select the most adequate threshold for a certain quantity. A possible solution, which would avoid some degree of arbitrariness, is the adoption of the root-mean-square of the considered quantities.
Nevertheless, in the present work we employed the same thresholds as those already adopted in the literature and, for the additional types of structures, we have shown that the thresholds proposed above yield adequate percolation curves.

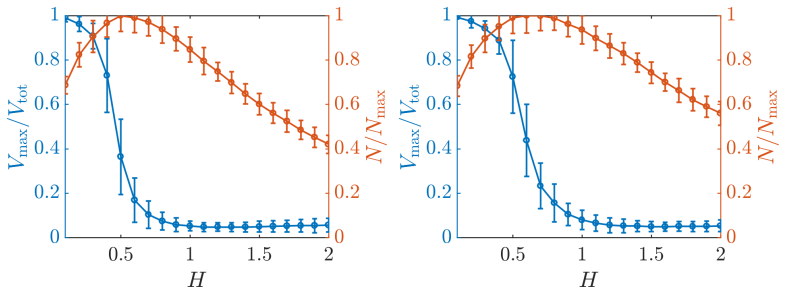

Figure 6. Percolation analysis for uv structures obtained with two different threshold functions: (left) $|uv| > H''_{uv}/2(u^2_{rms}+v^2_{rms})$ and (right) $|uv| > H''_{uv}/2(u^2_{rms}+v^2_{rms}+w^2_{rms})$.

3. Results and discussion

3.1. Structure classification

In their numerical studies of turbulent channel flows, del Álamo *et al.* [6] and Lozano-Durán *et al.* [7] reported the existence of different families of structures with respect with their shape and distances from the wall. More precisely, considering the joint probability density function of their minimum and maximum distances from the wall, it is possible to identify: 1) small objects located far from the walls, denoted in the following as detached (D); 2) small objects near the wall, denoted as wall-attached (WA); 3) large objects attached to the wall which extend beyond the centerline of the channel, referred to as tall-wall-attached (TWA). In both studies a "near-wall" region, defined below $y^+ = 20$, was used to classify the various structures.
In duct flows, because of the geometry, it is possible to identify at least seven analogous types

of structures: 1) detached (D), far from all the walls; 2) wall-attached (WA), close to at least one of the horizontal walls; 3) tall-wall-attached (TWA), elongated in the vertical direction and attached to the horizontal walls; 4) side-attached (SA), close to one of the vertical walls; 5) tall-side-attached (TSA), elongated in the horizontal direction and attached to at least one of the vertical wall; 6) corner-attached (CA), which are simultaneously close to both a horizontal and a vertical wall; 7) tall-corner-attached (TCA), which are large structures attached simultaneously to at least a horizontal and a vertical wall. In the present work, four near-wall regions are defined as $z^+, y^+ < 20$, evaluated based on the local value of Re_τ, and the classification is based on the wall-normal distance to the closest wall of the structures, and on the location of their center of mass. The center of mass is defined as $\mathbf{r}_{\rm cm} = \sum \Delta V_i \mathbf{r}_i$, where $\mathbf{r}_i$ is the position of the ith grid point belonging to the structure, and ΔV_i is the volume of the hexaedron the faces of which are orthogonal to the edges departing from the ith node and passing through their midpoints. Tall objects considered close to the walls (WA, SA and CA) have the coordinates of the center of mass $z_{\rm cm}$, $y_{\rm cm}$ located inside the near-wall regions. Objects consider attached to the walls (TWA, TSA and TCA) have the coordinates of the center of mass located outside the near-wall regions, but at least one point in the near-wall regions. Detached objects have no points in the near-wall regions. The criteria are summarized in Table 1 and illustrated in Figure 7 (left). Since the threshold is determined regardless of the classification into different families,

Table 1. Conditions for the classification of structures into different families, $y^+_{\rm nw} = z^+_{\rm nw} = 20$.

D	$y^+_{\rm min} > y^+_{\rm nw}$	&	$y^+_{\rm cm} > y^+_{\rm nw}$	&	$z^+_{\rm min} > z^+_{\rm nw}$	&	$z^+_{\rm cm} > z^+_{\rm nw}$
WA	$y^+_{\rm min} < y^+_{\rm nw}$	&	$y^+_{\rm cm} < y^+_{\rm nw}$	&	$z^+_{\rm min} > z^+_{\rm nw}$	&	$z^+_{\rm cm} > z^+_{\rm nw}$
TWA	$y^+_{\rm min} < y^+_{\rm nw}$	&	$y^+_{\rm cm} > y^+_{\rm nw}$	&	$z^+_{\rm min} > z^+_{\rm nw}$	&	$z^+_{\rm cm} > z^+_{\rm nw}$
SA	$y^+_{\rm min} > y^+_{\rm nw}$	&	$y^+_{\rm cm} > y^+_{\rm nw}$	&	$z^+_{\rm min} < z^+_{\rm nw}$	&	$z^+_{\rm cm} < z^+_{\rm nw}$
TSA	$y^+_{\rm min} > y^+_{\rm nw}$	&	$y^+_{\rm cm} > y^+_{\rm nw}$	&	$z^+_{\rm min} < z^+_{\rm nw}$	&	$z^+_{\rm cm} > z^+_{\rm nw}$
CA	$y^+_{\rm min} < y^+_{\rm nw}$	&	$y^+_{\rm cm} < y^+_{\rm nw}$	&	$z^+_{\rm min} < z^+_{\rm nw}$	&	$z^+_{\rm cm} < z^+_{\rm nw}$
TCA	$y^+_{\rm min} < y^+_{\rm nw}$	&	$y^+_{\rm cm} > y^+_{\rm nw}$	&	$z^+_{\rm min} < z^+_{\rm nw}$	&	$z^+_{\rm cm} > z^+_{\rm nw}$

it is interesting to assess the impact of the threshold on such classification. Figure 7 (Right) shows a slice of the uv field together with the connected components identified for three different values of H. The effect of a variation of H is quite complex: structures may disappear (1); they may remarkably change their volume without splitting (2); they may split into new structures, which may or may not belong to the same family (3); they may change family (4) and they may remain almost unchanged (5). Figure 8 shows the percentage of volume for the different families as a function of H for uv, uw and vw structures. It can be observed how the horizontal walls play the same role for uv events as that of the vertical walls for uw events, and vice-versa. Similarly, all the walls are equivalent for vw, $v^2 - w^2$ and K structures (note that only the first ones are shown), which is consistent with the symmetry of the case. For $H \simeq 1$, which is the value that maximizes the number of objects, TCA structures occupy most of the volume. Note that the distinction between horizontal and vertical walls for the square duct may appear unnecessary, but it has been maintained because objects such as uv and uw have a different role depending on which the nearest wall is: SA and TSA uv events are cross-flow events with respect to the vertical walls, and vice-versa for uw. Moreover, this subdivision allows to assess whether the sample size is large enough to reflect the statistical symmetry between uv and uw events, and it will be certainly needed in future comparisons with turbulent rectangular duct cases (Ref. [4]).

A comprehensive overview of how the various types of structures are subdivided into different

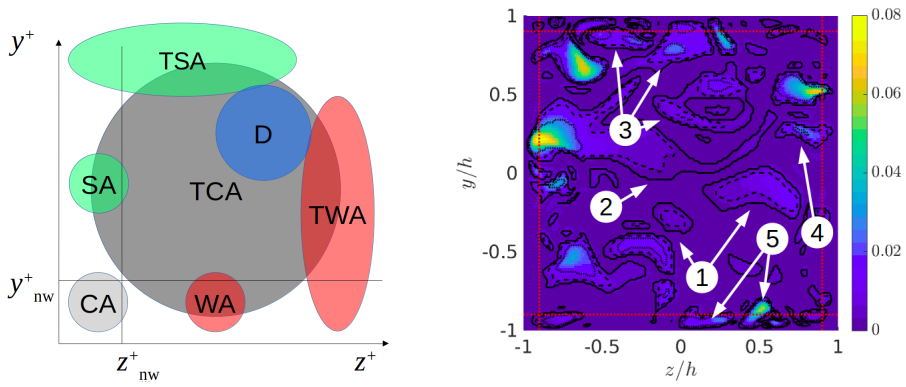

Figure 7. (Left) Sketch of the different families defined in Table 1 and (right) slice of a $|uv|$ field at a certain stramwise position in one of snapshots of the dataset. Solid, dashed and dotted lines represent connected components for $H = 0.5$, $H = 1$ and $H = 2$, respectively. The numbers from 1 to 5 represent the different phenomena observed when changing H described in the text. The dotted red lines are $y^+_{\rm nw}$ and $z^+_{\rm nw}$ defined at the centreplane.

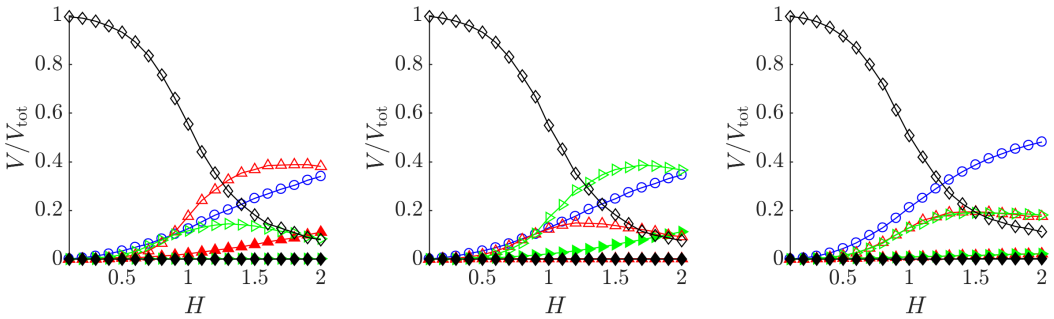

Figure 8. Volume occupied by each family over the total occupied volume as function of the thershold H, from (left) uv, (center) uw and (right) vw structures. The different families are denoted as follows: ○ detached (D), ▲ wall-attached (WA), △ tall wall-attached (TWA), ▶ side-attached (SA), ▷ tall side-attached (TSA), ♦ corner attached (CA) and ◊ tall-corner attached (TCA).

families is provided in Table 2. The corresponding fractions for $|uv|$ events in channel flow at $Re_\tau = 180$ are also reported for comparison. In all the cases, the volume of a specific structures is defined as the volume of the bounding box. In turbulent channel flows, as already reported in Ref. [7, 18] at Re_τ values from 930 to 4200, D events are the most numerous but they occupy a relatively small volume, whereas the majority of the volume is occupied by TWA events. Interestingly, in the duct most of the volume is occupied by TCA for all the considered types of structures, although the proportions among families are different depending on the structure under consideration. In particular, the fraction of the total volume occupied by the TCA is around 65% for uv and uw structures but below 50% for both $v^2 - w^2$ and K. The uncertainty of this result can be estimated by considering the discrepancy between values which are supposed to be identical due to the symmetry, and based on the results in Table 2 this uncertainty is of the order of 1%. The discrepancies among types of structures suggest the existence of qualitative differences in the shape and/or in the spatial organization of the various considered events,

Table 2. (Left) Fraction of the number of objects and (right) of the total volume of the objects. In both tables, $|uv|_{ch}$ are from channel flow.

	$\|uv\|_{ch}$	$\|uv\|$	$\|uw\|$	$\|vw\|$	$\|v^2-w^2\|$	K	$\|uv\|_{ch}$	$\|uv\|$	$\|uw\|$	$\|vw\|$	$\|v^2-w^2\|$	K
D	0.47	0.53	0.52	0.53	0.57	0.48	0.12	0.06	0.06	0.12	0.17	0.16
WA	0.23	0.11	0.05	0.10	0.08	0.12	0.01	0.01	$\simeq 0$	0.01	0.01	0.01
SA	–	0.05	0.12	0.10	0.08	0.13	–	$\simeq 0$	0.01	0.01	0.01	0.01
TWA	0.29	0.10	0.11	0.10	0.09	0.09	0.87	0.16	0.11	0.14	0.18	0.17
TSA	–	0.11	0.10	0.10	0.09	0.09	–	0.11	0.15	0.14	0.18	0.17
CA	–	0.03	0.03	0.02	0.02	0.02	–	$\simeq 0$	$\simeq 0$	$\simeq 0$	$\simeq 0$	$\simeq 0$
TCA	–	0.07	0.07	0.05	0.06	0.07	–	0.65	0.66	0.58	0.44	0.47

which might be related with the different role that they have in the dynamics of the flow. A comprehensive assessment of the various types of structures will be conducted in future work and in the following we focus on the uv events.

3.2. Characterization of uv structures

As already mentioned, the v and w velocity components are equivalent (with respect to the corresponding vertical or horizontal wall) in the square duct due to symmetry, and this is also the case with the uv and uw structures. Thus, it is possible to employ a coordinate transformation to account for both types of structures jointly when computing statistics. Note that uv structures in the duct correspond to uv structures in the channel only if they are located close to the horizontal walls (WA and TWA families), while they correspond to uw structures in the channel if they are close to the vertical walls (SA and TSA families). The correspondence is less obvious in the case of structures which are near the corners of the duct (CA), attached to a horizontal and a vertical wall (TCA) or far from them (D). It can be difficult to compare the size and shape of the structures in ducts and channels, even for equivalent families, because of the different geometry. In del Álamo *et al.* [6] and Lozano-Durán *et al.* [7], the structures are scaled in inner units, based on the wall-averaged friction velocity. In duct flows the presence of two orthogonal walls needs to be taken into account, and we proceed as follows: 1) the sizes of each structure is scaled with $\tilde{Re}_\tau(y,z)$, which is defined as an average of the Re_τ values based on the closest horizontal and vertical walls weighted with the corresponding distances to those walls; 2) the structures are grouped into a total of three different *regions*, based on the distance of their respective centers of mass $\mathbf{r}_{\rm cm}$ to the closest vertical wall, as shown in Figure 9 (left). Region (a) extends from the vertical walls up to the spanwise coordinate where Re_τ is almost constant (*i.e.* $1 > |z/h| > 0.7$), regions (b) and (c) are located closer to the duct vertical centerplane (at $0.7 > |z/h| > 0.4$ and $0.4 > |z/h| > 0$, respectively). This subdivision has the rationale of distinguishing uv events in the core of the duct, where structures exhibit closer similarity with the channel, from uv events near the vertical walls. Although the choice of these specific regions is arbitrary, it yields reasonable results as discussed below. On the one hand, it is not possible to estimate a priori where – and even *if* – the influence of the vertical walls on the structures becomes negligible, a fact that precludes from establishing a simple subdivision into two regions based on the spanwise location. On the other hand, a finer partitioning was not practical due to the resulting low number of objects in certain regions, and such a fine subdivision is in fact not necessary for the aim of the present work. The size of the structure bounding box in viscous units are defined Δx^+, Δy^+ and Δz^+, according to the frame of reference in the duct. The probability density function (PDF) of Δ_x^+ and Δ_y^+ in the three different regions of the duct are shown in Figure 9 (center) and (right), respectively. In these figures we compare the PDF obtained from

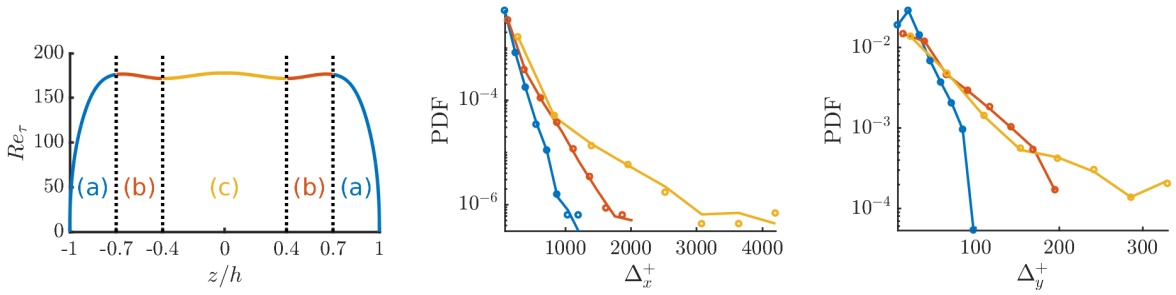

Figure 9. (Left) Distribution of Re_τ for the horizontal wall, where the letters and vertical dotted lines denote the three regions into which the structures are grouped).(Center) Normalized PDF of the inner-scaled structure sizes in the x and (right) in the y coordinates for the three regions. Solid lines and dots denotes PDFs computed based on the entire dataset and on half of the dataset, respectively.

all the instantaneous fields in the dataset (solid lines) and from half of the snapshots (dots). The good agreement between both indicates that the sample spaces under consideration in the present study ensures statistical convergence.

In order to compare the characteristics of the various families, Δ_y^+ and Δ_z^+ are represented as functions of Δ_x^+, in the sense that a convenient binning is adopted for Δ_x^+ and for each bin the averages $\langle\Delta_y^+\rangle$ and $\langle\Delta_z^+\rangle$ are computed, together with their standard deviation within the bin. Figure 10 shows a comparison of the families that are fully equivalent in channel and duct flows, *i.e.* D, WA, and TWA. Note that despite the remarkable agreement of the second-order fit with the trends observed in some of the considered cases, the fit was added only for visualization purposes, without any deeper physical implication in the context of the present work.

For the sake of brevity, in the following we will denote with a subscript the considered region, so that for instance the detached objects in region (a) of the duct are denoted as $\mathrm{D}_{(\mathrm{a})}$, and the detached objects of the channel are referred to as D_{ch}. It is possible to observe appreciable differences among families and, occasionally, among objects which belong to the same family but are located in different regions. The family $\mathrm{D}_{(\mathrm{a})}$ exhibits essentially the same behavior as that of D_{ch}, which is also consistent with $\mathrm{D}_{(\mathrm{b})}$ (albeit this region contains structures that, for the same streamwise length, are shorter and narrower), whereas $\mathrm{D}_{(\mathrm{c})}$ includes objects which are significantly shorter in both wall-normal directions. The subdivision into different regions of the duct is less relevant for WA structures, with $\mathrm{WA}_{(\mathrm{a})}$, $\mathrm{WA}_{(\mathrm{b})}$ and $\mathrm{WA}_{(\mathrm{c})}$ exhibiting similar features reasonably consistent with those of the WA_{ch} objects. Note that for the shorter structures, the channel exhibits objects with larger Δ_y^+ and Δ_z^+ values, a fact that could be connected with the constraining effect of the side walls in the duct. On the other hand, all the three $\mathrm{TWA}_{(\mathrm{a})}$, $\mathrm{TWA}_{(\mathrm{b})}$ and $\mathrm{TWA}_{(\mathrm{c})}$ families of structures have statistically significant differences for the longest objects, and only $\mathrm{TWA}_{(\mathrm{a})}$ exhibits a trend similar to that of TWA_{ch}, although with slightly smaller objects in the y and z directions for the same streamwise length. Interestingly, there are not any TWA structures in the duct that is large enough to reach both the horizontal walls. Regarding the duct, the identified structures are generally smaller if closer to the vertical walls, the only exception being the for $\mathrm{WA}_{(\mathrm{b})}$ and $\mathrm{WA}_{(\mathrm{c})}$, which are basically identical. Figure 11 shows the same size curves for of the CA and TCA families, which do not have a natural equivalent in channel flow due to the spanwise periodicity. Here, they are compared with WA_{ch} and TWA_{ch}, which are considered to be the closest equivalents if only uv structures are taken into account. CA structures are generally smaller than WA_{ch}, although they exhibit similar aspect ratios (which can be defined as the slopes of the Δ_y^+ and the Δ_z^+ curves) up to $\Delta_x^+ \simeq 200$,

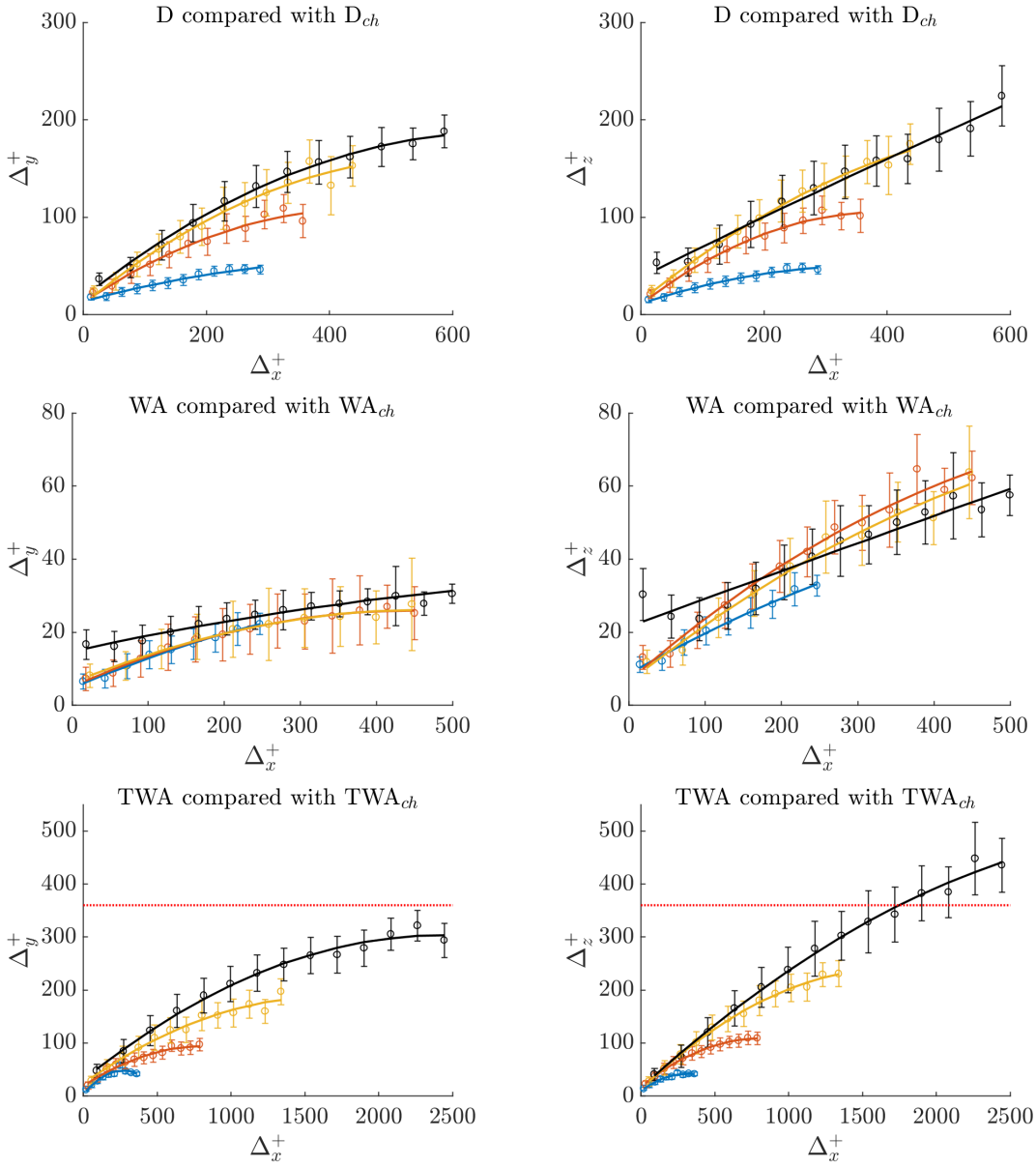

Figure 10. (Left) vertical size Δ_y^+ and (right) horizontal size Δ_z^+ as function of Δ_x^+ (in viscous units), for *uv* structures of the following families: from top to bottom, detached (D), wall-attached (WA) and tall-wall-attached (TWA). Blue, red and yellow are structures located in regions (a), (b) and (c) of the duct, consistently with Figure 9, and black is for structures of the corresponding families in channel flows. The solid lines in the figures are the results of a least-square fit with a second degree polynomial. The dotted red horizontal line represents the size of the domain for the duct.

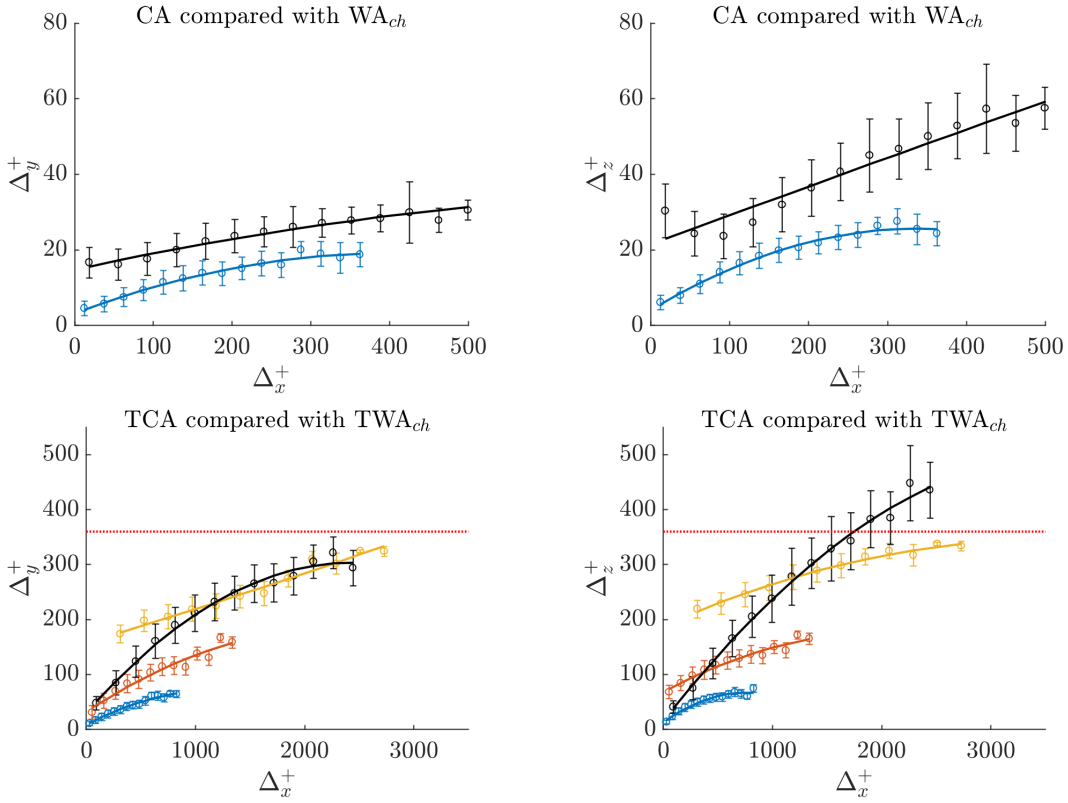

Figure 11. (Left) vertical size Δ_y^+ and (right) horizontal size Δ_z^+ as function of Δ_x^+ (in viscous units), for uv structures of the following families: from top to bottom, corner-attached (CA) and tall-corner-attached (TCA) in the duct, compared with wall-attached (WA) and tall-wall-attached (TWA) in the channel. Color code as in Figure 10.

while the TCA curves show a more complex behavior. The TCA$_{(a)}$ and TCA$_{(b)}$ families exhibit lower aspect ratios than the TWA$_{ch}$, and their trends are similar to the ones observed for the TWA$_{(a)}$ and TWA$_{(b)}$ families. The largest structures in the TCA$_{(c)}$ family are as tall and wide as the whole duct and when they occur they occupy most of transversal section of the duct, eventually being attached to all the walls.
The observation that the largest TWA$_{(c)}$ objects reach (and exceed) half of the width of the duct, together with the results summarized in Table 2 regarding the distribution of volume fraction for different families, suggest to consider the TCA and TWA families combined. These results are shown in Figure 12, which shows that the size in the y direction of the joint family TWA$_{(c)}$+TCA$_{(c)}$ is consistent with that of the TCA$_{ch}$ family for all the lengths, and up $\Delta_z^+ \simeq 300$ and $\Delta_x^+ \simeq 2000$ in the z direction.
The behavior of the remaining families, namely SA and TSA, has been studied but further analysis will be carried out, including a detailed comparison with the uw structures in the channel, and it will be reported in future publications.

4. Conclusions and outlook

The present study is aimed at a first characterization of coherent structures in turbulent square duct flows. By applying a percolation analysis to select a threshold function that maximizes the number of detected objects, intense events associated with five different quantities have

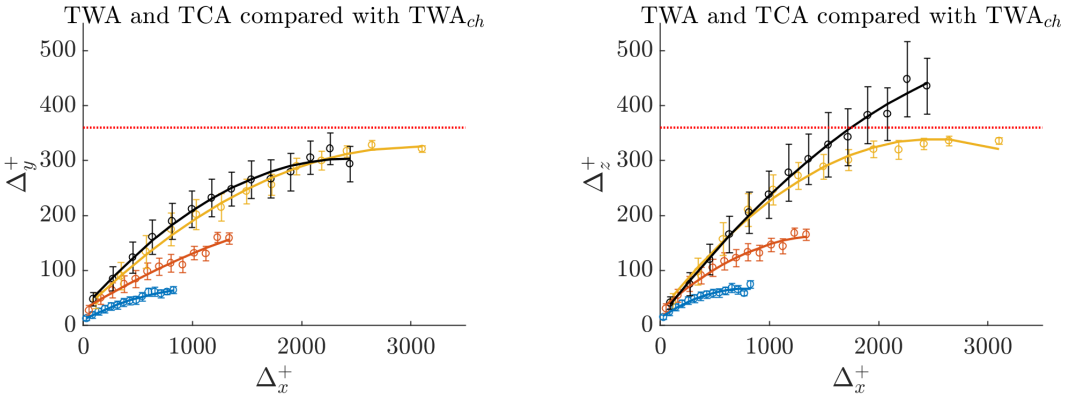

Figure 12. (Left) vertical size Δ_y^+ and (right) horizontal size Δ_z^+ as function of Δ_x^+ (in viscous units), for the uv structures in the duct, if the tall-wall-attached and tall-corner-attached families are considered jointly, compared with tall-wall-attached in the channel. Color code as in Figure 11.

been identified: uv, uw, vw, $v^2 - w^2$ and $K = (\tilde{v}^2 + \tilde{w}^2)/2$. The last three events have not been analyzed before with this percolation methodology, and our initial results show that their division into families with respect to the distance from the walls is similar but not identical to the results observed in uv structures. A more detailed study regarding the shape and size of the structures is reported for uv events, including a comparison with turbulent channel flow at similar a Re_τ of 180. Our main findings can be summarized as follows: 1) small uv structures attached to the wall are almost identical in the two cases (channel and duct); 2) the same is true for detached objects in the spanwise core of the duct, for which the presence of the vertical walls appears to have a negligible influence; 3) both detached structures close to the side wall and tall structures attached with the horizontal wall in the duct, are narrower than the same structures of the same streamwise length in the channel as approaching the vertical walls. The longest structures from these families in the duct are shorter in the streamwise direction than the equivalent ones in the channel; 4) when considered together, tall structures attached to the horizontal wall and tall objects attached to both the horizontal and vertical walls, if located near the spanwise centerplane the duct, have statistically the same size in y as that of the tall objects attached to the wall in the channel. Regarding their extent in z, the agreement between the duct and the channel is excellent up to $\Delta_z^+ \simeq 180$ (which is half of the total inner-scaled width of the duct), point after which the spanwise extent of the structures in the duct is smaller than that in the channel, with a maximum Δ_z^+ smaller than 360 (the total inner-scaled duct width). Finally, it is interesting to note how the different behavior of the various families can be clearly observed, despite the relatively low Re under consideration. These results constitute the starting point of additional studies to analyze the relations among the three-dimensional structures of different types and their role in the dynamics of flow.

Another area where additional studies are required is the percolation analysis. Firstly, it is necessary to investigate in detail whether it is possible to prescribe the threshold function with a more rigorous procedure. Indeed, if on the one hand it is possible to define different thresholds that guarantee the percolation crisis to occur for the same physical quantity, on the other hand the analogy between the threshold function and the application of a scaling suggests that it could be possible to establish the threshold based on physical arguments. Secondly, it is important to assess whether the percolation behavior is a universal feature of fully-developed turbulent flow and in this case if it is possible to extract physical insight from it. The remarkable agreement

with the simple test case of the square lattice raises the question of whether the percolation behavior is only a consequence of the chaotic appearance of turbulence or not. Contrary to the example of the random lattice, for turbulent flows it is expected to have a range of the sizes of coherent structures which increases with the Re due to the larger scale separation. This pictures is undoubtedly charming since it naturally fits with the concept of turbulent cascade. However, varying *ad hoc* parameters such as H leads to the fact that the connected components expand through all the domain due to the definition of percolation, a fact which poses the impelling question of whether the *very* large structures observed in both duct and channel flows are really physical objects or only artifacts of a too generous detection technique. These aspects will be further investigated in the future.

Acknowledgments

This study was funded in part by the Coturb program of the European Research Council. MA acknowledges funding from the Swedish Foundation for Strategic Research, project "In-Situ Big Data Analysis for Flow and Climate Simulations" (ref. number BD15-0082). RV and PS acknowledge the funding provided by the Swedish Research Council (VR) and from the Knut and Alice Wallenberg Foundation. We are grateful to Davide Modesti for his careful reviewing of the manuscript.

References

[1] Huser, A and Biringen, S 1993 *J. Fluid Mech.* **257** 65–95
[2] Gavrilakis, S 1992 *J. Fluid Mech.* **244** 101–129
[3] Pinelli, A, Uhlmann, M, Sekimoto, A and Kawahara, G 2010 *J. Fluid Mech.* **644,** 107–122
[4] Vinuesa, R Noorani, A, Lozano-Durán, A, El Khoury, G K, Schlatter, P, Fisher, P and Nagib, HM 2014 *J. Turbul.* **15** 677–706
[5] Vinuesa, R, Prus, C, Schlatter, P and Nagib, HM 2016 *Meccanica* **51** 3025–3042
[6] del Álamo, JC, Jiménez, J, Zandonade, P and Moser, RD 2006 *J. Fluid Mech.* **561** 329–358
[7] Lozano-Durán, A, Flores, O and Jiménez, J 2012 *J. Fluid Mech.* **694** 100–130
[8] Hunt, JCR, Wray, AA and Moin, P 1988 *Center Turbul. Res., Proc. Summer Prog. 1988* 193–208
[9] Jeong, J and Hussain, F 1995 *J. Fluid Mech.* **285** 69–94
[10] Chong, MS, Perry, AE and Cantwell, BJ 1990 *Phys. Fluids* **2** 765–777
[11] Chakraborty, P, Balachandar, S and Adrian, R J 2005 *J. Fluid Mech.* **535** 189–2014
[12] Chong, MS, Soria, J, Perry, AE, Chacin, J, Na, Y, and Cantwell, BJ 1996 *Center Turbul. Res., Proc. Summer Prog. 1996* 383–408
[13] Nagaosa, R and Handler, R A 2003 *Phys. Fluids* **15** 375–394
[14] Moisy, F and Jiménez, J 2004 *J. Fluid Mech.* **513** 111–133
[15] Wallace, JM, Eckelman, H and Brodkey, R S 1992 *J. Fluid Mech.* **54** 39–48
[16] Willmarth, WW and Lu, SS 1972 *J. Fluid Mech.* **55** 65–92
[17] Lu, SS and Willmarth, WW, 1973 *J. Fluid Mech.* **60** 481–511
[18] Lozano-Durán, A and Jiménez J 2014 *J. Fluid Mech.* **759** 432–471
[19] Vinuesa, R, Schlatter, P and Nagib, HM 2015 *Int. Symp. Turbul. Shear Flow Phenomena (TSFP-9)* pp 1–6